Actin Motion on Microlithographically Functionalized Myosin Surfaces and Tracks

Dan V. Nicolau,* Hitoshi Suzuki,# Shinro Mashiko,# Takahisa Taguchi,* and Susumu Yoshikawa*
*Osaka National Research Institute, Osaka 563, and #Kansai Advanced Research Center, Communications Research Laboratories, Kobe 651-2401, Japan

ABSTRACT High-resolution e-beam patterning exposure of the surface of poly[(*tert*-butyl-methacrylate)-*co*-(methyl methacrylate)]—a common e-beam and deep-UV resist used in semiconductor microlithography—induced sharp changes in the surface hydrophobicity. These differences in hydrophobicity resulted in the selective attachment of heavy meromyosin to hydrophobic, unexposed surfaces. The movement of the actin filaments on myosin-rich and myosin-poor surfaces was statistically characterized in terms of velocity, acceleration, and angle of movement. The actin filaments have a smooth motion on myosin-rich surfaces and an uneven motion on myosin-poor surfaces. Interestingly, an excess of myosin sites has a slowing, albeit mild effect on the motion of the actin filaments. It was also found that the myosin-rich/myosin-poor boundary has an alignment-enforcement effect, especially for the filaments approaching the border from the myosin-rich side. Based on these results, we discuss the feasibility of building purposefully designed molecular motor arrays and the testing of the hypotheses regarding the functioning of the molecular motors.

INTRODUCTION

The application of the semiconductor technology in experimental biomedical sciences has gained momentum in recent years. One stream of this synergism has evolved around the development of biomicrotechnologies. *Microlithographic-like technologies* are used for a light-assisted combinatorial chemistry technique (pioneered by Fodor et al., 1991) to build high-density peptide libraries (Gallup et al., 1994) and oligonucleotide arrays (McGall et al., 1996). Along this line of development, we reported the use of *microlithographic materials* as functionalized scaffolds for building protein and peptide structures (Nicolau et al., 1998, 1999).

The synergy between semiconductor technology and experimental biomedical sciences also led to a second stream of development focused on biodevice fabrication. Although *static* biodevices (e.g., biosensors, reviewed by Nicolini, 1995; and Fishman et al., 1998) have been developed for decades, only recently have the operation and fabrication of *dynamic* biomolecular devices been investigated. The operational aspects have been addressed by the study of the motion of individual kinesin molecules along microtubules using either optical trapping techniques (Funatsu et al., 1997; Higuchi et al., 1997; Kojima et al., 1997) or scanning probe force microscopy (Tokunaga et al., 1997). On the other hand, the fabrication of dynamic bimolecular devices that control the movement of kinesin molecular motors or actin filaments has been attempted, using microlithographic techniques to either fabricate silane patterns to which tubules selectively bind (Turner et al., 1995) or to fabricate poly(methyl methacrylate) profiled tracks to which myosin selectively binds (Suzuki et al. 1997), respectively.

At the confluence of these two streams of development, this work attempts to use radiation-assisted surface functionalization of a common microlithographic material with the objective of delivering a technique that may provide new insight into the mechanism of molecular motors.

MATERIALS AND METHODS

Preparation of protein-selective polymer surfaces

The radiation-sensitive material used in this study is a copolymer of *tert*-butyl-methacrylate (*t*BuMA) with methyl methacrylate (MMA). The copolymer P(*t*BuMA-*co*-MMA) was synthesized as described earlier (Nicolau et al., 1998b). The copolymer, with a *t*BuMA:MMA ratio of ~4:1, is sensitive to the e-beam radiation and deep-UV light. Four-inch silicon wafers were 1) liquid-primed with hexamethyldisilazane (purchased from Aldrich Co.); 2) spin-coated with a 5% polymer solution at a rotation speed of 3000 rpm to form uniform films ~0.6 μm thick; 3) soft-baked at 85°C in a convection oven for 3 h; and 4) pattern-exposed with an e-beam exposure machine (ZBA 21; Jenoptik, Jena, Germany), using a test pattern with an exposure energy of ~5 μC/cm^2. The wafers were cut into 1-cm^2 squares to accommodate the further processes of the selective attachment of the proteins. A protein solution, either of fluorescein isothiocyanate (FITC) avidin for pattern visualization, or of heavy meromyosin for control of the movement of actin filaments, was deposited on the surface of the patterned exposed resist. The protein patterning procedure is presented in Fig. 1. The proteins attach preferentially to hydrophobic, unexposed areas. A sample of the FITC avidin pattern is presented in Fig. 2.

Surface characterization

The surface of the P(*t*BuMA-*co*-MMA) films prepared as described above was exposed to e-beam radiation with energies varying from 1 to 50 μC/cm^2. The contact angle of 0.5-μl water drops deposited on unexposed, partially exposed, and fully exposed P(*t*BuMA-*co*-MMA) surfaces was measured with a Kyowa Kagaku Co. anglemeter. The change in the atomic

Received for publication 6 November 1998 and in final form 28 April 1999.
Address reprint requests to Dr. Dan V. Nicolau, RioTinto/Research and Technology Development, Locked Bag 347, Bentley Delivery Centre, WA 6983, Perth, Australia. Tel.: +61-894707828; Fax: +61-894705579; E-mail: dan.nicolau@riotinto.com.au.

0006-3495/99/08/1126/09 $2.00

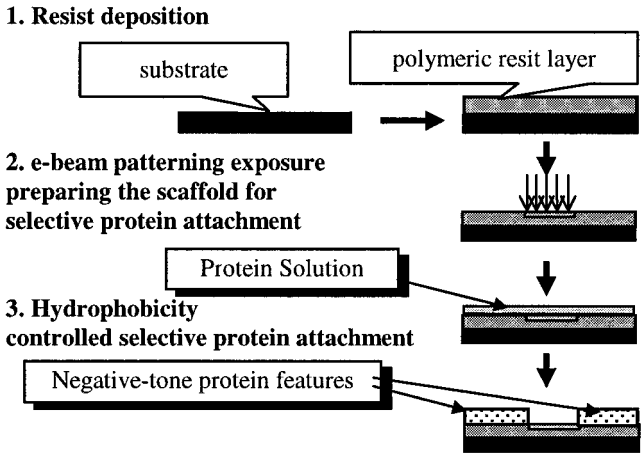

FIGURE 1 Technological steps for the patterning of proteins via negative tone e-beam lithography. The exposed regions become hydrophilic and inhibit the protein attachment to the polymer surface.

concentration of the oxygen on the resist surface versus exposure energy was measured with an ESCA spectrometer (Escascope; VG Scientific).

Motility assay

The procedures of the motility assay were described previously (Suzuki et al., 1995, 1997). Briefly, heavy meromyosin (HMM) and actin were extracted from the back and leg muscle of a rabbit and purified by methods previously reported (Margossian and Lowey, 1982; Pardee and Spudich, 1982). The actin filament was labeled with tetramethyl-rhodamine-phalloidin for fluorescence observation. The assay buffer solution used in the experiment consisted of 40 mM KCl, 3 mM $MgCl_2$, 2 mM EGTA, 10 mM dithiothreitol (DTT), and 20 mM HEPES (pH 7.8).

Experimental setup for observation

The patterned P(*t*BuMA-*co*-MMA) resist surface was used as a scaffold for protein selective attachment. The observation cell consists of a glass coverslip on which the 1-cm^2 piece of silicon wafer with the patterned polymer surface on top was fixed with an adhesive and a nitrocellulose-coated coverslip. Two parallel lines of grease were placed on both sides of the silicon wafer as spacers for the buffer solution. A drop of a solution of HMM (0.1 mg/ml in the assay buffer) was placed on the surface of the patterned polymer, and then the cell was covered with the nitrocellulose-coated coverslip. HMM molecules were selectively adsorbed to the polymer surface during a 5-min contact time. Unbound HMM molecules were washed from the cell by infusing the assay buffer solution from one side of the cell. Finally the assay buffer solution containing actin filaments labeled with tetramethylrhodamine-phallodin, 1 mM ATP, 5 mg/ml glucose, 50 μg/ml glucose oxidase, and 10 μg/ml catalase was introduced into the cell.

Data collection and analysis

Actin filaments moving on the surface were observed at room temperature (24–25°C) with an epifluorescence microscope (Olympus BX-50) and recorded with an image-intensified CCD camera system (Hamamatsu Photonics C2400-87) and a Hi-8 VCR set (Sony EV-NS7000NTSC). The recorded images were further processed and statistically analyzed using an image analysis software (Retrac, University of York, UK). Data collection consisted of recording 20 consecutive incremental positions of 20 and 30 actin filaments moving on myosin-rich and myosin-poor surfaces, respectively. The frequency of image collection was 10 frames/s. The coordinates of the consecutive positions were used to compute the instantaneous velocity, acceleration, angle of movement, and alignment of the movement compared with the direction between hydrophobic and hydrophilic regions.

RESULTS AND DISCUSSION

Radiation-induced changes of the polymeric surface

The surface oxygen content of the P(*t*BuMA-*co*-MMA) increased slightly from 61.47% to 64.47%. The radiation-induced changes in surface hydrophobicity are presented in Fig. 3. Overall, the hydrophilization of the P(*t*BuMA-*co*-MMA) surface continues with the increase in the exposure energy, but with a much slower rate after reaching an exposure energy of ~15 μC/cm^2. The surface contact angle varies in the range 90°–75° according to the exposure en-

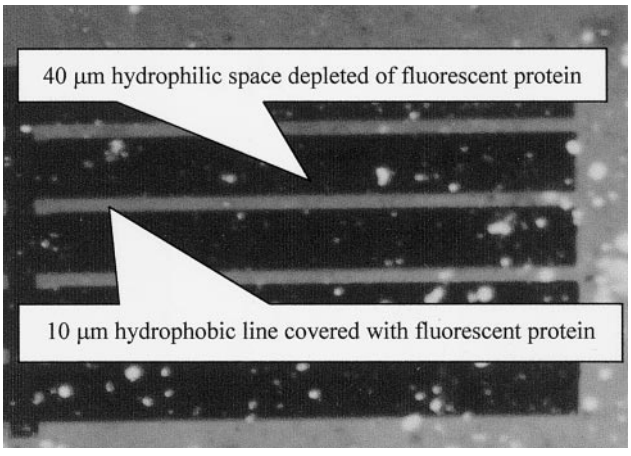

FIGURE 2 Protein (FITC avidin) features printed on the surface of a P(*t*BuMA-*co*-MMA) resist via e-beam lithography. Only scattered globular protein agglomerates are present on hydrophilic regions, whereas a continuous protein blanket is present on hydrophilic tracks.

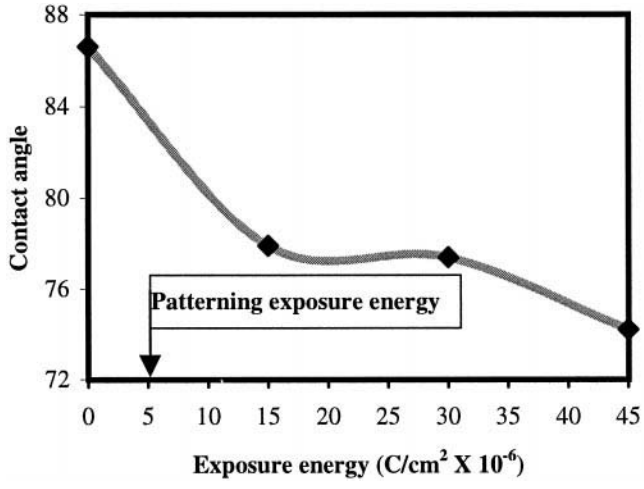

FIGURE 3 Evolution of surface hydrophobicity (contact angle) with exposure energy (μC/cm^2) for a P(*t*BuMA-*co*-MMA) resist. The patterning exposure used low energies to minimize the effect of reactions that do not contribute to the change in surface hydrophobicity.

ergy. The experiments for determining the relationship between the e-beam exposure energy and the hydrophobicity of the polymer surface are tedious, and corroborating experimental evidence from the microlithography literature (e.g., Miller and Brault, 1981) is readily available. Hence the hydrophobicity as a function of exposure energy was probed only at four points.

The radiation-induced changes in the surface properties are consistent with the mechanism proposed in Fig. 4 (*left column*). Briefly, for low exposure energies only the *t*BuMA moieties react to form carboxylic groups, with a slight increase in the oxygen content relative to the carbon content, but an important increase in surface hydrophilicity. In the high vacuum conditions of the e-beam exposure, the *tert*-butyl alcohol is totally desorbed from the polymer surface. At high exposure energies the main reaction is depolymerization (not presented in Fig. 4). Because depolymerization induces moderate changes in surface hydrophobicity (Fig. 3, higher exposure energies) and because high exposure energy might also induce the permeabilization of the polymer surface, only low exposure energies are recommended.

Based on 1) the fact that the maximum variation in hydrophobicity occurs between 0 and 15 $\mu C/cm^2$; 2) only the surface (as opposed to bulk) chemistry is relevant for this study; and 3) previous extensive microlithographic experience (e.g., Miller and Brault, 1981), we chose 5 $\mu C/cm^2$ as the patterning exposure energy.

Building actin-sensitive polymer surfaces

The sharp contrast in the hydrophobicity of the e-beam-sensitive copolymer versus exposure energy allowed the selective attachment of the HMM without the need for the selective dissolution of the exposed resist (as described by Suzuki et al., 1997). The procedure used in this study (presented in Fig. 1) offers the following potential advantages: 1) a simpler patterning process (i.e., no need for complex microlithograhic techniques, as described by Turner et al., 1995); 2) versatility, as P(*t*BuMA-*co*-MMA) is a common microlithographic material, sensitive to both e-beam (Miller and Brault, 1981) and deep-UV light (Allen et al., 1994); 3) avoidance of the risk of contamination with organic solvents (used for selective dissolution, as presented by Suzuki at al., 1997); and, most importantly, 4) the opportunity to study the movement of the actin filaments free from extraneous mechanical constraints (associated with profiled surfaces, as in Suzuki at al., 1997).

The protein features (as in Fig. 2) were printed on the unexposed areas of the P(*t*BuMA-*co*-MMA) resist. The mechanism proposed for the selective attachment of protein to unexposed resist areas is presented in Fig. 4 (*right column*). The contrast of the HMM images was assessed via inspection of the FITC avidin images (Fig. 2). On hydrophilic regions fluorescent light manifests as a shift toward higher wavelengths. This effect was observed in a previous work (Nicolau et al. 1998a) when we printed FITC avidin on hydrophilic regions, using a different material (diazonaphto-quinone/novolak) and a different printing mechanism (attachment via amide linkage between protein amino groups and photogenerated carboxylic groups).

Although the attachment response of the HMM versus surface hydrophobicity might be different from the attachment response of the avidin, a high selectivity is expected to occur in a region of steep response of the hydrophobicity versus exposure energy, i.e., around the same exposure

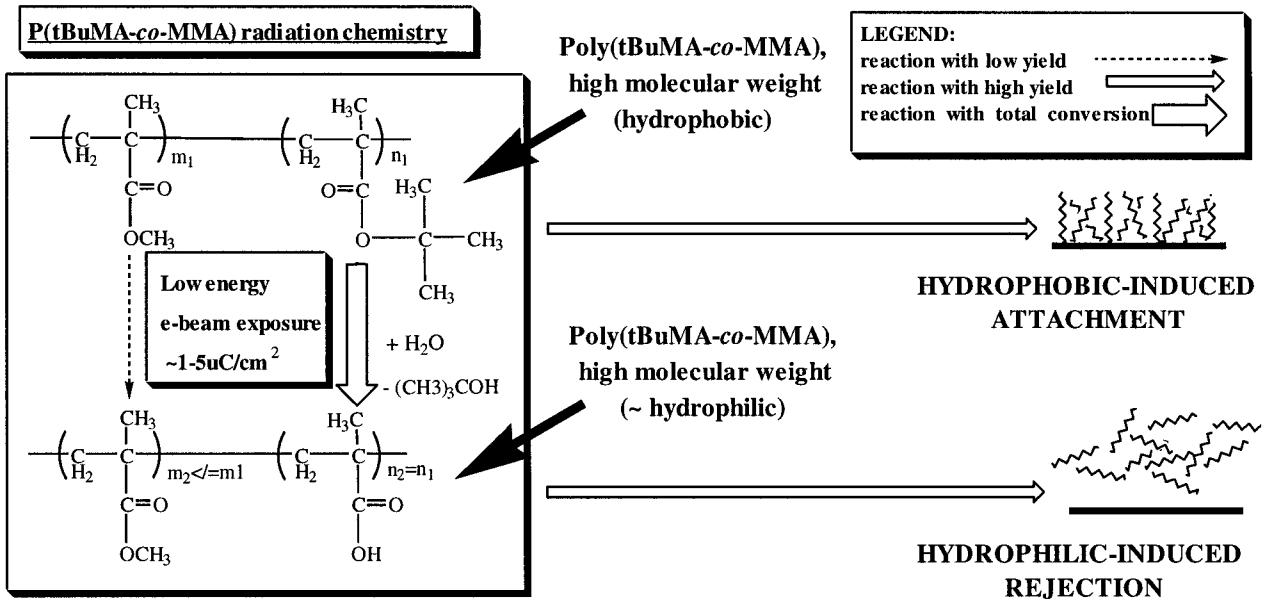

FIGURE 4 The mechanism resposible for heavy meromyosin attachment on an e-beam resist surface. For low exposure energies the depolymerization of the polymer is suppressed (i.e., $m_2 \approx m_1$ and $n_2 \approx n_1$, *left-hand side*), but the yield of generation of carboxylic groups on the surface, and hence the selectivity of protein attachment (*right-hand side*), is high.

energy. Consequently, the hydrophobic surfaces were designated as myosin-rich, and hydrophilic surfaces as myosin-poor. A more detailed account regarding the attachment selectivity of the proteins on hydrophobic, unexposed resist surfaces versus exposed, hydrophilic ones was presented (Nicolau et al., 1999).

Contrast of the images of the fluorescent actin filaments

The hydrophilic environment of the exposed surfaces induces a decrease in the apparent fluorescence of the actin filaments due to the influence of the environment on the quantum yield (e.g., Lakowicz, 1983). Consequently, the statistical analysis of the image data had to use a statistical sampling ~50% larger on hydrophilic/myosin-poor regions than the one used for the hydrophobic/myosin-rich surfaces, to counterbalance the loss of image clarity. A snapshot of the actin filaments moving on hydrophobic and hydrophilic areas is presented in Fig. 5.

Characteristics of the motion of the actin filaments

To assess the different behavior of the actin filaments on polymer surfaces with different HMM concentrations, we defined several characteristic measures of the filaments' motion. The velocity, acceleration, and angle are used to assess the different types of motion on myosin-poor and myosin-rich regions. The alignment of the movement with respect to the boundary between myosin-poor and myosin-rich regions is a measure of the capacity to confine the filaments on microlithographically functionalized myosin tracks. The definitions of the motion characteristics are presented in Fig. 6. The velocity was computed using two sequential positions; computation of the acceleration and the angle required three sequential positions. The alignment required three sequential positions and the direction defined by the myosin-rich/myosin-poor boundary.

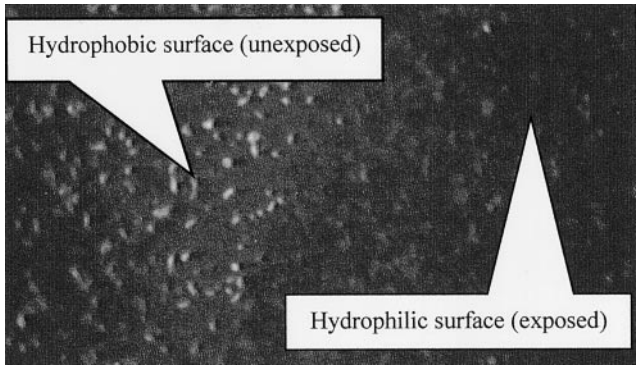

FIGURE 5 Difference in the fluorescence of the actin filaments (rhodamine) on hydrophilic ("myosin-poor") and hydrophobic ("myosin-rich") polymer surfaces.

Behavior of the actin filaments on myosin-rich and myosin-poor surfaces

The motion of the actin on surfaces with different hydrophobicities and, consequently, different HMM concentrations has the following characteristics:

The *average velocity* of the actin filaments on the myosin-rich surface is ~10% lower than the velocity on the myosin-poor one (i.e., mean value of 3.66 μm/s versus 4.03 μm/s, respectively).

The *frequency distribution* of the *velocity* of the actin filaments (*histograms* presented in Fig. 7 *A*) on the myosin-rich area is steeper than on the myosin-poor one (i.e., a standard deviation of 0.92 versus 1.19, respectively).

The *average acceleration* of the actin filaments is, as expected, close to zero on both the myosin-rich and myosin-poor surfaces (i.e., mean values of -0.04 μm/s^2 and -0.09 μm/s^2, respectively). This suggests a representative statistical sampling.

The *frequency distribution* of the *acceleration* of the actin filaments (Fig. 7 *B*) on the myosin-rich surface is again more narrow than on the myosin-poor one (i.e., a standard deviation of 1.31 versus 1.72, respectively).

The *average angle of motion* of the actin filaments is closer to 180° on myosin-rich surfaces than on myosin-poor ones (i.e., mean values of 157° and 137°, respectively).

The *frequency distribution of the angle of motion* (Fig. 7 *C*) shows that the filaments on a myosin-rich surface are more likely to preserve a linear motion (i.e., the distribution is almost entirely confined to angles varying between 145° and 180°) than the filaments moving on myosin-rich surface (which have a flatter distribution, with a sizable occurrence at angles below 145° and even at angles around 70°). Again, the standard deviation of the angle is lower on myosin-rich surfaces than on myosin-poor ones (24° and 37°, respectively).

Behavior of the actin filaments at the myosin-rich/myosin-poor boundary

The motion of the actin filaments on narrow hydrophobic lines (Fig. 8) tends to be confined to the lines. In Fig. 8 the trajectories of the actin filaments are rainbow-color-coded, i.e., red corresponds to the initial position, the colors around green correspond to the medium positions, and purple corresponds to the last position in a motion sequence. The actin filaments on myosin-rich lines tend to be "reflected" when approaching the myosin-rich/myosin-poor boundary. The trajectories on the myosin-poor region are mildly "attracted" to the myosin-rich region when approaching the boundary. The statistical analysis shows that the motion of the actin filaments near the myosin-rich/myosin-poor boundary presents the following characteristics:

The *spatial distribution of the velocity* near the myosin-rich/myosin-poor boundary shows again that the frequency distribution of the velocities on the hydrophobic, myosin-rich lines (in the region between -5 and 0 μm on the x axis in Fig. 9 *A*) is tighter. In contrast, the velocities are largely

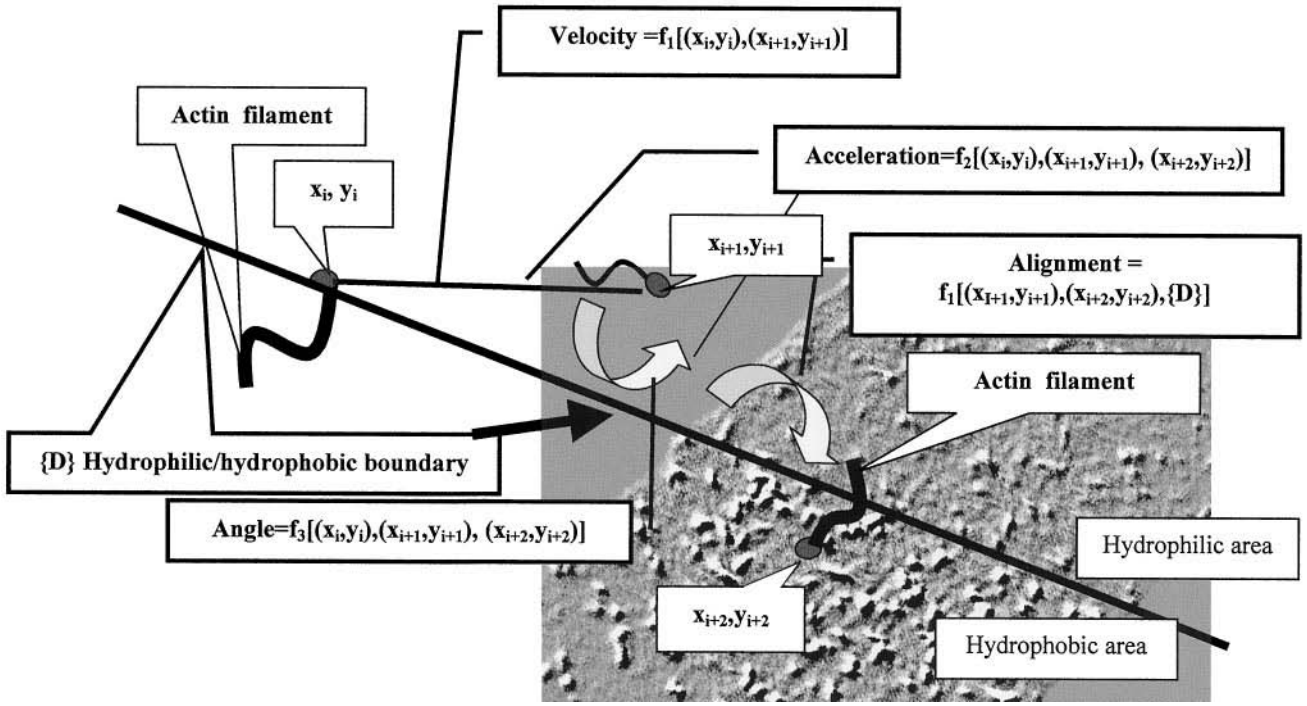

FIGURE 6 Definitions of the velocity, acceleration, angle, and alignment of the movement of the actin filaments. The positions of the actin filament, crossing the hydrophobic/hydrophilic boundary two times in three steps, are marked as (x_i, y_i), (x_{i+1}, y_{i+1}), and (x_{i+2}, y_{i+2}) for the initial, middle, and last positions, respectively. The inset represents an image of the filaments close to the myosin-rich/myosin-poor boundary.

distributed on the hydrophilic, myosin-poor region, especially far (i.e., beyond 15 μm) from the boundary. Finally, the actin filaments "aggregate" in a distinct statistical population near the border.

The *spatial distribution of the acceleration* (Fig. 9 *B*) is almost perfectly centered on 0 on both myosin-rich and myosin-poor regions (proving that the statistical sampling is representative). The null value for the mean acceleration is visualized better for the latter because of less statistical interference far from the boundary). Interestingly, there is a noticeable, positive accelerated motion on the myosin-poor area in the immediate vicinity of the boundary. This can be explained if we assume that the filaments approaching the hydrophobic area are "attracted" (i.e., accelerated), whereas the filaments approaching the border from the hydrophobic area are "deflected" (i.e., decelerated). Furthermore, the effect seems to be a boundary-induced one, as the average velocity of the actin filaments is slightly larger on myosin-poor regions than on myosin-rich ones (the acceleration should be negative when passing from a higher velocity to a lower one).

The *spatial distribution of the angle of motion* (Fig. 9 *C*; only nontrivial values below 160° are presented) is, for values around 180°-150°, largely independent of the location of the actin filaments, i.e., on the myosin-rich or myosin-poor regions. However, for the lower angles, the effect of the confinement near the boundary becomes evident. Although about the same proportion of filaments can turn through 60° in both myosin-rich and myosin-poor areas (i.e., *far from the border, at the extreme left and extreme right* in Fig. 9 *C*), the angles of motion are restricted to values around 100° and higher at the myosin-rich/myosin-poor boundary (0 on the *x* axis). Moreover, the confinement is more apparent on the hydrophobic side, accounting for the gradual deflection and the walking along the boundary of the actin filaments on the myosin-rich lines (as shown in Fig. 8). The actin filaments coming toward the myosin-rich line from the myosin-poor region are not deflected, but rather are mildly "attracted," resulting in a weaker confinement of the motion.

The *spatial distribution of the alignment* of the motion (Fig. 9 *D*) shows that the movement of the actin filaments is, within statistical error, aligned with the axis of the myosin-rich line. The frequency distribution of the angle of deflection (i.e., deviation from a perfect alignment) is grouped around 20° in the myosin-rich area and closer to the myosin-rich/myosin-poor boundary, whereas the distribution of the alignment angle is random in the myosin-poor area and far from the boundary (i.e., at the *extreme right* in Fig. 9 *D*).

Mechanisms of motion of the actin filaments on surfaces with different myosin concentrations

Other researchers (Andreev et al., 1995) have investigated the influence of the myosin concentration on actin's behavior. It was found that the orientation of the myosin heads on F-actin is dependent on the density of heads (i.e., on the

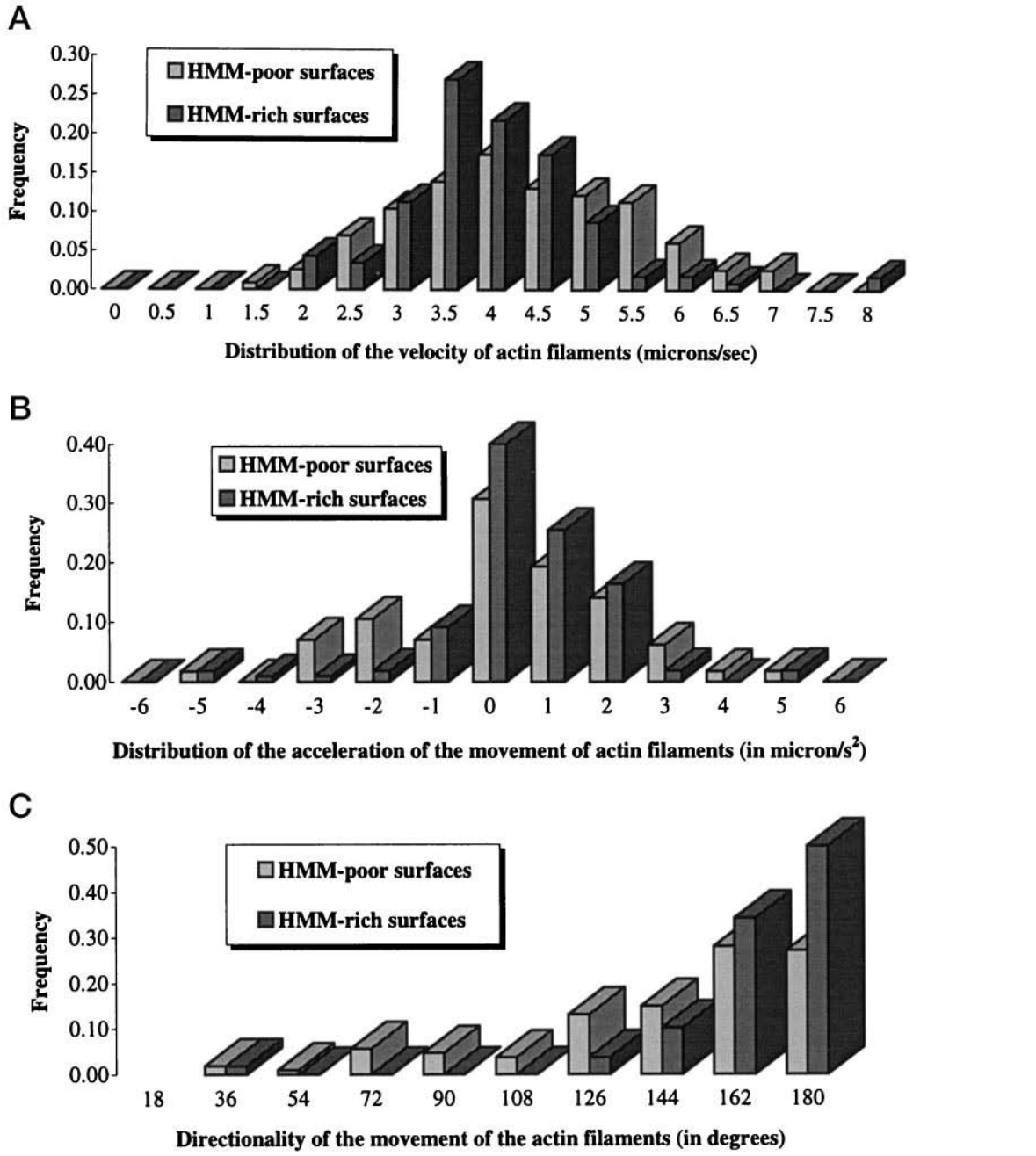

FIGURE 7 Histograms of the characteristics of the actin filament motion on HMM-poor and HMM-rich surfaces, respectively, as frequency distribution of respective (*A*) velocities, (*B*) accelerations, and (*C*) angles.

saturation of available sites on the actin filaments). To present a method for the further study of molecular motors and to assess the feasibility of manufacturing artificial dynamic devices, we studied the influence of the surface density of myosin on actin filament movement from a global, "engineering" perspective.

On the basis of our observations (outlined above), the likely mechanism of the movement of the actin filaments on myosin-rich and myosin-poor regions and at the boundary between regions with different myosin concentrations can be summarized as follows:

On *myosin-rich surfaces* the actin filaments have unrestricted and instantaneous access to myosin sites, resulting in a smooth motion. The smoothness of the motion is supported by 1) a narrow distribution of the velocity (Fig. 7 *A*); 2) a narrow distribution of the acceleration and a mean value close to zero, i.e., constant velocity (Fig. 7 *B*); and 3) the preservation of the motion directionality (a narrow distribution of the angles of motion grouped around 180°, as in Fig. 7 *C*).

On *myosin-poor surfaces* the actin filaments have restricted access to less dense myosin sites, resulting in a more

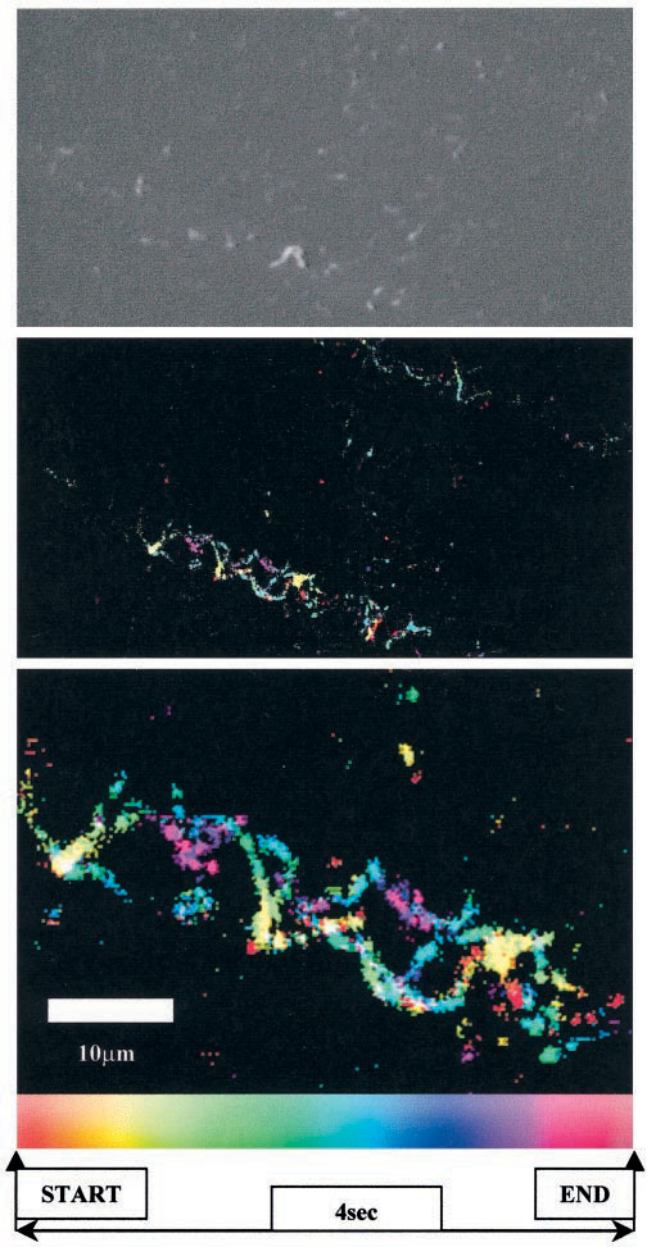

FIGURE 8 Partial confinement of the movement of the actin filaments on myosin-rich lines. The photographs represent a snapshot of the movement of the actin filaments (*top*), an overlap of 20 sequential positions (*middle*), and a 3× enlargement (*bottom*). The positions of the actin filaments on the last two photographs were color-coded, as explained by the gauge at the bottom of the figure.

uneven motion, supported by 1) a broader distribution of the velocity than the one on myosin-rich regions (Fig. 7 *A*); 2) a broader distribution of the accelerations (Fig. 7 *B*); and 3) a broader distribution of the angle of movement (Fig. 7 *C*).

The *boundary between myosin-rich and myosin-poor regions* has an alignment-enforcement effect (evident in Figs. 8 and 9 *D*). This effect is more pronounced for the actin filaments approaching the boundary from the myosin-rich region, because these filaments have a substantially higher propensity to remain on the originating surface than the filaments moving on myosin-poor surfaces. The alignment effect of the myosin-rich/myosin-poor boundary can be explained by the higher preference of the actin filaments for myosin-rich surfaces when presented with the choice of myosin-rich or myosin-poor regions. When this choice is not available (i.e., far from the boundary), on either myosin-rich or myosin-poor areas, the alignment effect disappears entirely (as presented by the broader distribution of the alignment of the movement far from the boundary in Fig. 9 *A*).

Interestingly, a higher concentration of myosin sites seems to have a slowing, albeit mild effect on the motion of the actin filaments. This can be understood if we assume that the actin filaments have a subtly different mechanism of motion on myosin-rich and myosin-poor surfaces, respectively. On myosin-rich regions, an excess of myosin may induce a faster but short-range motion of the segments of the actin filaments. At a more global level, the segments may visit myosin sites adjacent to the main trajectory of the filament, resulting in a sinuous motion of the filament. This sinuous motion may slightly delay the overall velocity of the filament, despite the propensity for the preservation of the linearity of the motion of the front of the filament. The opposite mechanism may occur on myosin-poor regions, where the actin filaments have a straighter long-range motion between less dense myosin sites.

No "trapping" effect of the actin filaments on myosin-rich regions has been observed. We assume that the system operated far from an energy-starvation point, in terms of both ATP concentration and temperature. Energy-starved systems, which would increase the capability to control the motion of mobile elements, will be investigated in the future.

Artificial dynamic devices based on protein molecular motors

The building of these devices would benefit from 1) a higher control of the motion of the motile components (e.g., actin filaments in this study); 2) a selective mechanism that controls the in-phase motion directionality (i.e., ideally all mobile elements moving in the same direction and sense); 3) a rationalization of the tasks that can be performed by the dynamic device. Building on previously reported literature (Turner et al., 1995; Suzuki et al., 1997) and on the present study, some possible lines of research are proposed as follows.

The *control of the motion of the mobile components* could be achieved via:

Higher selectivity of the density of the motors on the surface. A higher selectivity would require specifically designed polymers with steeper hydrophobicity response versus exposure or more selective protein attachment mechanisms (e.g., selective chemical linkage on radiation-induced chemical sites—as proposed by Nicolau et al., 1999—instead of hydrophobicity-controlled HMM attachment).

Higher resolution of the selectively functionalized tracks, i.e., narrower and better designed tracks. The present study

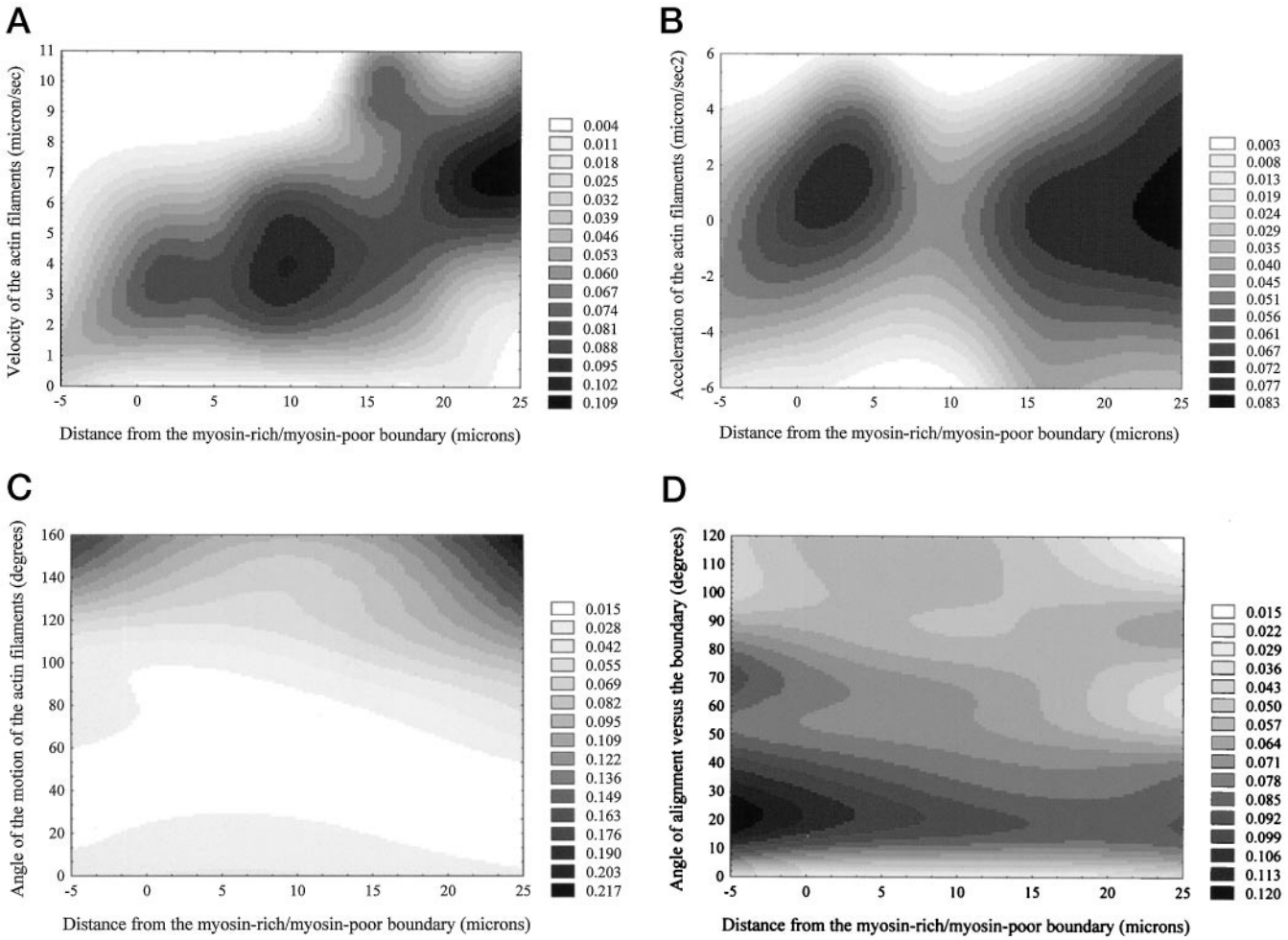

FIGURE 9 Statistics of actin filament movements near the boundary between hydrophobic and hydrophilic regions, as spatial distribution of velocities (*A*), acceleration (*B*), angle (*C*), and alignment (*d*), versus distance from the myosin-rich/myosin-poor boundary.

suggests that the confinement of the motion is more effective near the myosin-rich/myosin-poor boundary, and possibly better on curved tracks. Larger mobile elements would ease the restrictions placed on very high resolution lithography. More importantly, more rigid mobile elements (e.g., microtubules) may be conducive to a more effective control of the motion.

The use of built-in mechanical confinement, e.g., channel-profiled features instead of flat surfaces (as in this study and Turner et al., 1995) and hill-profiled features (as in Suzuki et al., 1997).

A *modus operandi* closer to the threshold of the energetic starvation of the system, using controlled lower concentrations of ATP and/or lower temperatures.

A *mechanism controlling the in-phase motion directionality* could be achieved via

The design of molecular selectors, possibly linked in series, using the frequency distribution of the mobile elements versus obligated angles of motion.

The use of external mechanical confinement, e.g., magnetic fields for the mobile elements labeled with magnetic beads, or fluid flow (Ostap et al., 1992) for the mobile elements labeled with large molecular "sails" (as recently proposed by Turner et al., 1995).

At the molecular level, the *tasks performed by the dynamic device* could be:

to transfer *mechanical energy*, e.g., movement of the tip of an atomic force microscope in a ratchet-type mechanism;

to transform *mechanical energy into electrical energy*, e.g., either in an "electrical generator" mode or in an "electrical motor" mode, via the controlled movement of a magnetic bead on top of microlithographically patterned metallic wires, or via the use of dipole interactions in microtubules for signal propagation (Brown and Tuszynski, 1997);

to transform *mechanical energy into optical energy*, via the manipulation of fluorescence in molecularly confined spaces or by using environment-induced effects.

The mechanics of molecular motors can be tested using microlithographically fabricated tracks functionalized with protein molecular motors as follows:

The *mechanics of collisions* can be tested via the study of the effects of the angle of collision and velocity on the

"splitting" or "coalescence" efficiency of the mobile elements (i.e., actin filaments or microtubules).

The *mechanics of bending* can be tested by studying the impact of the angle or the radius of the track curvature on the "kinetic energy" of the filament (i.e., velocity).

CONCLUSIONS

The present paper studies the different behavior of the movement of the actin filaments on microlithographically fabricated, myosin-functionalized surfaces. High-resolution e-beam patterning exposure of the surface of poly[(*tert*-butyl-methacrylate)-*co*-(methyl-methacrylate)] induced sharp changes in the surface hydrophobicity. These differences in hydrophobicity resulted in the selective attachment of heavy meromyosin to hydrophobic, unexposed surfaces. It was found that the actin filaments have a smooth versus uneven motion, in terms of velocity, directionality, and acceleration, on myosin-rich and myosin-poor surfaces, respectively. An excess of myosin has a slowing, albeit mild effect on the motion of actin filaments.

We thank Nick Carter from the Marie Curie Research Institute for the donation of his image analysis software; Kazuhiro Oiwa and Akira Yamada for the protein solutions preparation; and Cris dos Remedios and Robert Cross (from the University of Sydney and the Marie Curie Research Institute, respectively) for insightful discussions. One of the authors (DVN) wishes to acknowledge the Science and Technology Agency of Japan for partially supporting this work through a STA Fellowship and to thank his daughter, Alice, for first observing the differences in the movement of the actin filaments on different surfaces.

REFERENCES

Allen, R. D., G. M. Wallraff, W. D. Hinsberg, L. L. Simpson, and R. R. Kunz. 1994. Methacrylate terpolymer approach in the design of a family of chemically amplified positive resists. *In* Polymers for Microelectronics. ACS Symposium Series, Vol. 537. L. Thompson, C. G. Willson, and S. Tagawa, editors. American Chemical Society, Washington, DC. 155–167.

Andreev, O. A., R. Takashi, and J. Borejdo. 1995. Fluorescence polarization study of the rigor complexes formed at different degrees of saturation of actin filaments with myosin subfragment-1. *J. Muscle Res. Cell Motil.* 16:353–367.

Brown, J. A., and J. A. Tuszynski. 1997. Dipole interactions in axonal microtubules as a mechanism of signal propagation. *Phys. Rev. E.* 56:5834–5840.

Fishman, H. A., D. R. Greenwald, and R. N. Zare. 1998. Biosensors in chemical separations. *Annu. Rev. Biophys. Biomol. Struct.* 27:165–198.

Fodor, S. P. A., J. L. Read, M. C. Pirrung, L. Stryer, A. T. Lu, and D. Solas. 1991. Light-directed, spatially addressable parallel chemical synthesis. *Science.* 251:767–773.

Funatsu, T., Y. Harada, H. Higuchi, M. Tokunaga, K. Saito, Y. Ishii, R. D. Vale, and T. Yanagida. 1997. Imaging and nano-manipulation of single biomolecules. *Biophys. Chem.* 68:63–72.

Gallup, M. A., R. W. Barrett, W. J. Dower, S. P. A. Fodor, and E. M. Gordon. 1994. Applications of combinatorial technologies to drug discovery. 1. Background and peptide combinatorial libraries. *J. Med. Chem.* 37:1233–1251.

Higuchi, H., E. Muto, Y. Inoue, and T. Yanagida. 1997. Kinetics of force generation by single kinesin molecules activated by laser photolysis of caged ATP. *Proc. Natl. Acad. Sci. USA*. 94:4395–4400.

Kojima, H., E. Muto, H. Higuchi, and T. Yanagida. 1997. Mechanics of single kinesin molecules measured by optical trapping nanometry. *Biophys. J.* 73:2012–2022.

Lakowicz, R. 1983. Principle of Fluorescence Spectroscopy. Plenum Press, New York and London. 189–215.

Margossian, S. S., and S. Lowey. 1982. Preparation of myosin and its subfragments from rabbit skeletal muscle. *Methods Enzymol.* 85:55–71.

McGall, G., J. Labadie, P. Brock, G. Wallraff, T. Nguyen, and W. Hinsberg. 1996. Light-directed synthesis of high-density oligonucleotide arrays using semiconductor photoresists. *Proc. Natl. Acad. Sci. USA.* 93:13555–13560.

Miller, L. J., and R. G. Brault. 1981. A method for rapidly screening polymers as electron beam resists. *J. Electrochem. Soc.* 128:1158–1161.

Nicolau, D. V., T. Taguchi, H. Taniguchi, and S. Yoshikawa. 1998. Micron-size protein patterning using on diazo-naphto-quinone/novolak polymeric films. *Langmuir.* 14:1927–1936.

Nicolau, D. V., T. Taguchi, H. Taniguchi, and S. Yoshikawa. 1999. Positive and negative tone protein patterning using conventional deep-UV/e-beam resists. *Langmuir*. 15:3845–3851.

Nicolini, C. 1995. From neural chip and engineered biomolecules to bioelectronic devices: an overview. *Biosens. Bioelectron.* 10:105–127.

Ostap, E. M., T. Yanagida, and D. D. Thomas. 1992. Orientational distribution of spin-labeled actin oriented by flow. *Biophys. J.* 63:966–975.

Pardee, J. D., and J. A. Spudich. 1982. Purification of muscle actin. *Methods Enzymol.* 85:164–181.

Suzuki, H., K. Oiwa, A. Yamada, H. Sakakibara, H. Nakayama, and S. Mashiko. 1995. Linear arrangement of motor protein on a mechanically deposited fluoropolymer thin film. *Jpn. J. Appl. Phys.* 34:3937–3941.

Suzuki, H., A. Yamada, K. Oiwa, H. Nakayama, and S. Mashiko. 1997. Control of actin moving trajectory by patterned poly(methylmethacrylate) tracks. *Biophys. J.* 72:1997–2001.

Tokunaga, M., T. Aoki, M. Hiroshima, K. Kitamura, and T. Yanagida. 1997. Subpiconewton intermolecular force microscopy. *Biochem. Biophys. Res. Commun.* 231:566–569.

Turner, D. C., C. Chang, K. Fang, S. L. Brandow, and D. B. Murphy. 1995. Selective adhesion of functional microtubules to patterned silane surfaces. *Biophys. J.* 69:2782–2789.